J. Fluid Mech. (1974), *vol.* 63, *part* 4, *pp.* 695–721
Printed in Great Britain

Finite-amplitude thermal convection in a spherical shell

By RICHARD E. YOUNG

Advanced Study Program, National Center for Atmospheric Research,
Boulder, Colorado 80302†

(Received 12 September 1973)

The properties of finite-amplitude thermal convection for a Boussinesq fluid contained in a spherical shell are investigated. All nonlinear terms are retained in the equations, and both axisymmetric and non-axisymmetric solutions are studied. The velocity is expanded in terms of poloidal and toroidal vectors. Spherical surface harmonics resolve the horizontal structure of the flow, but finite differences are used in the vertical. With a few modifications, the transform method developed by Orszag (1970) is used to calculate the nonlinear terms, while Green's function techniques are applied to the poloidal equation and diffusion terms.

Axisymmetric solutions become unstable to non-axisymmetric perturbations at values of the Rayleigh number that depend on Prandtl number and shell thickness. However, even when stable, axisymmetric solutions are not a preferred solution to the full equations; steady non-axisymmetric solutions are obtained for the same parameter values. Initial conditions determine the characteristics of the finite-amplitude solutions, including, in the cases of non-axisymmetry, whether or not a steady state is achieved. Transitions in horizontal flow structure can occur, accompanied by a transition in functional dependence of heat flux on Rayleigh number. The dominant modes in the solutions are usually the modes most unstable to the onset of convection, but not always.

1. Introduction

Many important geophysical and astrophysical problems involve thermal convection in spherical geometries. Therefore, an understanding of how convective flow fields behave when curvature cannot be neglected seems essential in trying to comprehend these systems. This study is a numerical investigation of the finite-amplitude behaviour of a Boussinesq layer of fluid confined between two concentric spherical boundaries and heated from below. The boundaries are taken as free surfaces. Rotation is not considered here, because an understanding of the fluid dynamics in a stationary system is desirable before the considerable complications of rotation are imposed. In treating some geophysical or astrophysical situations, certain aspects of the problem as developed here, such as the Boussinesq approximation, would probably have to be modified.

† Present address: Space Science Division, NASA, Ames Research Center, Moffett Field, California 94035.

Nevertheless, the results obtained should yield valuable information on the kinds of flow behaviour that can occur.

The results of linear theory concerning the onset of convection for various spherical cases are reported in Chandrasekhar (1961). There it is shown that the critical Rayleigh number R_0, as defined in § 2, is in general a decreasing function of the ratio of inner to outer boundary radius, and is independent of the azimuthal wavenumber. These results assume the principle of exchange of stability. Computations of R_0 by Durney (1968), as well as those done in this study, indicate that this is a valid assumption for the present situation, since they agree with the R_0 determined by the formulae in Chandrasekhar.

Durney (1968) integrated the equations of motion for the above system using Herring's approximation, which neglects fluctuating nonlinear self-interactions. Herring's approximation allows the finite-amplitude solution to be given in terms of a single mode, when the solution is expanded in spherical suface harmonics. Durney demonstrated numerically that, when the ratio of inner boundary radius to outer boundary radius was 0·8 (the only case he considered), the stable finite-amplitude solution consisted of the mode most unstable to the onset of convection. For low Rayleigh numbers, this mode was the same as the one which maximized the heat flux.

In this paper, the complete nonlinear expressions for advection of temperature and momentum are retained in the equations, and both axisymmetric and non-axisymmetric solutions are investigated. The intent is not to conduct an extensive parametric survey (because, for one thing, the required computer time would be excessive). Rather, it is to examine interesting aspects of the finite-amplitude solutions. For example, in contrast to results using the Herring approximation, the dominant mode in the finite-amplitude solutions is not always the mode most unstable to the onset of convection. In addition, sudden transitions in both horizontal flow structure and dependence of heat flux on Rayleigh number can occur, and oscillatory behaviour is observed in certain instances as well.

Finally, there is a fundamental difference between the problem treated here and plane parallel convection (or, for that matter, spherical convection using the Herring approximation). The finite-amplitude solution completely determines the horizontal spectral character of the flow. *A priori* choice of horizontal wavenumber is no longer possible. This is, of course, a result of the fact we are considering a completely enclosed volume combined with nonlinear effects.

A formal statement of the problem is given in § 2, followed by a description of the numerical procedure in § 3. Sections 4 and 5 present the numerical results.

2. Detailed model

The basic model considered is that of a Boussinesq fluid contained in the region between two isothermal concentric spherical boundaries located at radii r_1 and r_2, r_1 being the inner boundary. The shell overlies a core of the same density as the fluid. The gravitational acceleration g is then given by

$$g = 4\pi G/r^2 \int_0^r \rho r^2 dr = \tfrac{4}{3}\pi G\rho r,$$

where ρ is the fluid density, r is the radius, G is the gravitational constant and the gravitational field is $-g\hat{\mathbf{r}}$. The problem is non-dimensionalized, using the distance between the boundaries d as the length scale, d^2/ν as the time scale, where ν is the kinematic viscosity, and ΔTP as the temperature scale, where ΔT is the applied temperature difference across the spherical shell, and $P = \nu/\kappa$, κ being the thermal diffusivity. The velocity is scaled with ν/d.

The dimensionless equations governing the fluid are

$$\frac{\partial}{\partial t}\nabla\times\mathbf{u}+\nabla\times[(\nabla\times\mathbf{u})\times\mathbf{u}] = \frac{R}{r_2}\nabla\times T\mathbf{r}+\nabla\times\nabla^2\mathbf{u}, \tag{2.1}$$

$$\nabla.\mathbf{u} = 0, \tag{2.2}$$

$$\frac{\partial T}{\partial t}+\mathbf{u}.\nabla T = \frac{1}{P}\nabla^2 T. \tag{2.3}$$

where $\mathbf{u}$ is the fluid velocity, T the temperature and the Rayleigh number

$$R = \frac{\alpha\Delta T g_0 d^3}{\kappa\nu}. \tag{2.4}$$

In (2.4) α is the coefficient of thermal expansion, and g_0 is the value of g at the outer boundary. The boundaries at r_1, $r_2\,(=r_1+1)$ will be taken as free surfaces. Thus, in a spherical co-ordinate system (r,θ,ϕ), where θ is the co-latitude,

$$u_r = \frac{\partial(u_\theta/r)}{\partial r} = \frac{\partial(u_\phi/r)}{\partial r} = 0 \quad \text{at} \quad r_1, r_2.$$

The fluid is heated from below so that the temperature in the absence of convection T_0 is

$$T_0 = -\frac{1}{P}\frac{(1-r_1/r)}{(1-r_1/r_2)}. \tag{2.5}$$

T_0 has been taken as zero at r_1. The total temperature T is the sum of $T_0(r)$ and the deviation from the purely conductive solution $\Theta(r,\theta,\phi,t)$. At r_1 and r_2, Θ vanishes.

Using the fact $\mathbf{u}$ is solenoidal, we shall write $\mathbf{u}$ in terms of poloidal and toroidal vectors (cf. Chandrasekhar 1961). Expanding in spherical surface harmonics $Y_L^m(\theta,\phi)$ with coefficients $t_L^m(r,t)$ and $p_L^m(r,t)$ for the toroidal and poloidal parts, respectively, gives

$$\left.\begin{aligned} u_r &= \sum_{L,m}\frac{L(L+1)}{r^2}p_L^m Y_L^m, \quad u_\theta = \sum_{L,m}\left[\frac{1}{r}\frac{\partial p_L^m}{\partial r}\frac{\partial Y_L^m}{\partial\theta}+\frac{t_L^m}{r\sin\theta}\frac{\partial Y_L^m}{\partial\phi}\right], \\ u_\phi &= \sum_{L,m}\left[\frac{1}{r\sin\theta}\frac{\partial p_L^m}{\partial r}\frac{\partial Y_L^m}{\partial\phi}-\frac{t_L^m}{r}\frac{\partial Y_L^m}{\partial\theta}\right]. \end{aligned}\right\} \tag{2.6}$$

Writing

$$\Theta = \sum_{L,m}\Theta_L^m(r,t)\,Y_L^m, \tag{2.7}$$

the equations for t_L^m and p_L^m are obtained by applying the operators $\hat{\mathbf{r}}.$ and $\hat{\mathbf{r}}.\,\mathrm{curl}$ o (2.1). Defining $S_L^m = p_L^m/r$ and $T_L^m = t_L^m/r^2$,

$$\frac{\partial T_L^m}{\partial t}-D_L T_L^m = -\frac{1}{L(L+1)}\{\hat{\mathbf{r}}.\nabla\times[(\nabla\times\mathbf{u})\times\mathbf{u}]\}_L^m, \tag{2.8}$$

$$\frac{\partial}{\partial t}\mathscr{D}_L S_L^m - \mathscr{D}_L^2 S_L^m = \frac{r}{L(L+1)}\left\{\hat{\mathbf{r}}.\nabla\times\nabla\times[(\nabla\times\mathbf{u})\times\mathbf{u}]\right\}_L^m - \frac{R}{r_2}\Theta_L^m, \tag{2.9}$$

$$\frac{\partial\Theta_L^m}{\partial t} - \frac{1}{P}\mathscr{D}_L\Theta_L^m = -\left\{\nabla.(\mathbf{u}T)\right\}_L^m, \tag{2.10}$$

where $$\mathscr{D}_L = \frac{d^2}{dr^2}+\frac{2}{r}\frac{d}{dr}-\frac{L(L+1)}{r^2}, \quad D_L = \frac{d^2}{dr^2}+\frac{4}{r}\frac{d}{dr}+\frac{2-L(L+1)}{r^2},$$

and $\{\}_L^m$ denotes the (L,m) component of the quantity within. The boundary conditions are

$$S_L^m = \frac{\partial^2 S_L^m}{\partial r^2} = \frac{\partial T_L^m}{\partial r} = \Theta_L^m = 0 \quad \text{at} \quad r_1, r_2. \tag{2.11}$$

The form of Y_L^m is chosen to agree with Condon & Shortley's (1951) definition of spherical harmonics, so that

$$Y_L^{m*} = (-1)^m Y_L^{-m}, \tag{2.12}$$

the star denoting the complex conjugate. In addition,

$$\int_0^{2\pi}\int_0^{\pi} Y_L^m Y_{L'}^{m'*}\sin\theta\, d\theta\, d\phi = \delta_{LL'}\delta_{mm'}. \tag{2.13}$$

To reduce the amount of computer time involved in the calculations by a factor of between 2 and 4, only hemispheric models are considered (i.e. u_θ is an odd function of θ about the equator, while all other variables are even functions). It can be seen from the governing equations that, if the initial conditions possess this symmetry about the equator, the subsequent solution will also. Poloidal and thermal modes are therefore restricted to modes with $L+m$ even, while the toroidal modes have $L+m$ odd. It should be noted that, if the initial conditions possess the opposite symmetry from that described above, the subsequent solution will not retain this symmetry, and both symmetric and antisymmetric modes would appear in the solution. The problem we are considering is rigorously equivalent to that of a hemispheric shell with the equatorial plane a thermally insulating boundary having zero tangential stress.

It is easy to show that in the steady state the sum of the conductive and convective heat flux,

$$-4\pi r^2\frac{d\bar{T}}{dr} + r^2\overline{u_r\Theta},$$

is independent of r. The bar denotes an integral over angles.

3. Numerical method

The basic structure of the numerical procedure is as follows. The problem is treated as a time-dependent initial-value problem. An expansion in terms of spherical surface harmonics is used for computing the horizontal variations of the flow fields, while in the radial direction a grid system is established instead of expanding in terms of radial eigenfunctions. Centred differences are used to approximate first- and second-order radial derivatives. As discussed later in § 3, second-order derivatives are the highest that had to be approximated.

The use of surface harmonics instead of finite differences to resolve the horizontal structure of the flow field has certain numerical advantages. The first is that special difficulties which occur near the poles in finite-difference methods (Holloway *et al.* 1973) are eliminated. Second, instabilities due to the aliasing errors of a horizontal grid do not exist (Orszag 1970). The reason for using a grid in the radial direction is that the appropriate radial functions for an expansion are combinations of spherical Bessel functions and powers of r, and no efficient means of calculating nonlinear coefficients was apparent.

Knowing the values of T_L^m, S_L^m, Θ_L^m at time t, the task is to find their values at time $t+\Delta t$, and so on. The first step in the process is to calculate the (L,m) coefficients of the nonlinear terms on the right-hand side of (2.8)–(2.10) at time t. The manner in which this is done is discussed later in § 3, and is the most time consuming part of the computation. After this has been completed, the next step is to consider (2.9). At first glance the left-hand side presents a problem. A fourth-order derivative appears, as well as the time derivative of spatial derivatives up to second order. Finite differencing the left-hand side would mean that a matrix equation would have to be solved for the values of S_L^m at $t+\Delta t$, and in order to avoid a time step restriction proportional to $(\Delta r)^4$, where Δr is the radial grid spacing, implicit methods would have to be used. The approximation of fourth- and third-order derivatives by finite differences did not appear desirable, because a fine grid would be necessary before such approximations would have any meaning.

The method employed here is to use a Green's function, G_L, for the operator $\mathscr{D}_L$, and then rewrite (2.9) as

$$\frac{\partial}{\partial t}S_L^m - \mathscr{D}_L S_L^m = \int_{r_1}^{r_2} r_0^2 G_L(r,r_0)\,(\text{RHS}\,(2.9))\,dr_0 + \left[r_0^2\frac{\partial G_L}{\partial r_0}\left(\frac{\partial S_L^m}{\partial t} - \mathscr{D}_L S_L^m\right)\right]\Bigg|_{r_1}^{r_2}, \tag{3.1}$$

where the boundary conditions on G_L have been chosen so that

$$G_L = 0 \quad \text{at} \quad r_1, r_2. \tag{3.2}$$

Equation (3.1) is derived as follows. Let $F = \partial S_L^m/\partial t - \mathscr{D}_L S_L^m$ and h equal the right-hand side of (2.9). Then

$$\left[\frac{d^2}{dr_0^2} + \frac{2}{r_0}\frac{d}{dr_0} - \frac{L(L+1)}{r_0^2}\right]F(r_0) = h(r_0). \tag{3.3}$$

The Green's function G_L satisfies

$$\left[\frac{d^2}{dr_0^2} + \frac{2}{r_0}\frac{d}{dr_0} - \frac{L(L+1)}{r_0^2}\right]G_L(r,r_0) = \frac{\delta(r-r_0)}{r_0^2}, \tag{3.4}$$

where $\delta(r-r_0)$ is the Dirac delta function. Multiplying (3.3) by $r_0^2 G_L$, (3.4) by $r_0^2 F$, subtracting and integrating the result over r_0 from r_1 to r_2 gives (3.1) when G_L satisfies (3.2). G_L is easily obtained, and is given by (see Jackson 1962, pp. 79–80)

$$G_L(r,r_0) = \frac{-1}{(2L+1)\left[1-(r_1/r_2)^{2L+1}\right]}\left(r_<^L - \frac{r_1^{2L+1}}{r_<^{L+1}}\right)\left(\frac{1}{r_<^{L+1}} - \frac{r_>^L}{r_2^{2L+1}}\right), \tag{3.5}$$

where $r_>$ ($r_<$) is the greater (lesser) of r or r_0. Using this Green's function approach also has the advantage that third-order derivatives occurring in the nonlinear terms can be integrated by parts, so that at no point in the numerical procedure do radial derivatives higher than second order have to be approximated by finite differences. The integral in (3.1) was approximated using the trapezoidal rule. The boundary values of the quantity

$$\partial S_L^m/\partial t - \mathscr{D}_L S_L^m$$

are simply $-(2/r)(dS_L^m/dr)$. Because $d^2S_L^m/dr^2 = 0$ at r_1, r_2, a one-sided difference gives dS_L^m/dr to $O(\Delta r^2)$.

The left-hand sides of (2.8), (2.10) and (3.1) could now be straightforwardly approximated by finite differences, using a leapfrog or some other appropriate scheme. However, a different method was chosen here for the following reasons. In all but the most nonlinear cases, the most stringent constraint on the time step is usually due to the second-order derivative occurring in the diffusion terms. Implicit methods, such as that of Crank–Nicholson, applied to the diffusion terms can eliminate the diffusive stability restriction on the time step, however, it is not likely that modes with wavelength the order of Δr would be appropriately represented, i.e. viscously damped, unless $\Delta t \lesssim \Delta r^2$. A desirable way to handle diffusion would be one that allows $\Delta t > \Delta r^2$, but at the same time retains the damping character. The use of the Green's function for the one-dimensional diffusion equation allows this to be done.

The procedure will be illustrated using the temperature equation (2.10), which is rewritten as

$$\frac{\partial \theta_L^m}{\partial t} - \frac{1}{P}\frac{\partial^2 \theta_L^m}{\partial r^2} = \text{RHS}\,(2.10) + \frac{2}{rP}\frac{\partial \theta_L^m}{\partial r} - \frac{L(L+1)}{r^2 P}\theta_L^m. \tag{3.6}$$

In most of the cases considered in this paper, the time step restriction in a finite-difference scheme resulting from the last two terms on the right side of (3.6) would be less stringent than that resulting from the second-order derivative on the left-hand side. By using the one-dimensional diffusion equation Green's function, the second-order radial derivative can be eliminated, and (3.6) becomes

$$\Theta_L^m(r, t+\Delta t) = \int_t^{t+\Delta t}\int_{r_1}^{r_2} G_{\Theta_L^m}[\text{RHS}\,(3.6)]\,dr_0\,dt_0 + \int_{r_1}^{r_2}[G_{\Theta_L^m}\Theta_L^m]\,|_t\,dr_0. \tag{3.7}$$

The Green's function involved in (3.7) can be obtained in closed form; however, a typical term would be proportional to

$$\exp\{(r-r_0)^2/4t\}.$$

It is readily seen that the number of operations required to perform the spatial integrals on such a term would be $O(N_r^2)$, where N_r is the number of vertical levels. The alternative is to use an eigenfunction expansion for the Green's function, which then gives (see Morse & Feshbach 1953)

$$G_{\Theta_L^m}(r, t|r_0, t_0) = 2\sum_{n=1}^{\infty}\exp\{-n^2\pi^2(t-t_0)/P\}\sin n\pi(r-r_1)\sin n\pi(r_0-r_1). \tag{3.8}$$

$G_{\Theta_L^m}$ has been chosen so that it vanishes at r_1, r_2. The Green's function for S_L^m is the same as $G_{\Theta_L^m}$, except the factor P does not appear in the exponential describing the time dependence. The expression for $G_{T_L^m}$ is

$$G_{T_L^m}(r,t|r_0,t_0) = 1+2\sum_{n=1}^{\infty}\exp\{-n^2\pi^2(t-t_0)\}\cos n\pi(r-r_1)\cos n\pi(r_0-r_1), \quad (3.9)$$

where $G_{T_L^m}$ is chosen so that $\partial G_{T_L^m}/\partial r = \partial G_{T_L^m}/\partial r_0 = 0$ at r_1, r_2. The boundary conditions satisfied by the Green's functions correspond to the boundary conditions satisfied by the respective variables. The highest term retained in the expansions (3.8) and (3.9) is $n = N_r$. Because of the expansion in trigonometric functions, fast Fourier transforms can be used in conjunction with the techniques described by Cooley *et al.* (1970) to perform the spatial integrations using the trapezoidal rule. Thus, the total number of operations required for integration and summing the modes (see below) is $O(N_r \log_2 N_r)$ for a given (L,m) mode. An implicit finite-difference scheme involving a tridiagonal matrix would require $O(4N_r)$ operations (Westlake 1968), and, as mentioned before, probably still require $\Delta t \lesssim \Delta r^2$. Clearly, the damping character of the diffusive terms is explicitly present in the Green's functions, and it can be shown from simple linear examples that, when the time integration is done as described below, no time step restriction proportional to $n^2\pi^2$ exists.

The spatial integrations in (3.8) and (3.9) are performed first, then the time integration. The function involved in the time integral besides the Green's function was approximated by a first-order Taylor series, e.g. letting f represent the function

$$f(t_0) \cong f|_t + \left.\frac{\partial f}{\partial t}\right|_t (t_0 - t). \quad (3.10)$$

The quantity $\partial f/\partial t$ was approximated by a one-sided backward difference in time. The time integral involving the exponentials in the Green's function can then be performed analytically, and, once this is done, the series is summed over n to obtain T_L^m, S_L^m, and Θ_L^m at time $t+\Delta t$. The series is summed over n because it is much quicker numerically to finite-difference the sum than to work with the coefficients of the trigonometric functions when computing the (L,m) components of the nonlinear terms. The calculation of the latter will now be considered.

In the appendix it is shown that the nonlinear terms involve three types of products of the spherical harmonics:

$$Y_{L_1}^{m_1} Y_{L_2}^{m_2}, \quad (3.11a)$$

$$\frac{1}{\sin\theta}\left[\frac{\partial Y_{L_1}^{m_1}}{\partial\theta}\frac{\partial Y_{L_2}^{m_2}}{\partial\phi} - \frac{\partial Y_{L_1}^{m_1}}{\partial\phi}\frac{\partial Y_{L_2}^{m_2}}{\partial\theta}\right], \quad (3.11b)$$

$$\frac{\partial Y_{L_1}^{m_1}}{\partial\theta}\frac{\partial Y_{L_2}^{m_2}}{\partial\theta} + \frac{1}{\sin^2\theta}\frac{\partial Y_{L_1}^{m_1}}{\partial\phi}\frac{\partial Y_{L_2}^{m_2}}{\partial\phi}. \quad (3.11c)$$

Defining

$$I^{a,b,c}(L,m,L_1,m_1,L_2,m_2) = \int_0^{2\pi}\int_0^{\pi} Y_L^m[\text{terms (3.11}a\text{–}c)]\sin\theta\, d\theta\, d\phi,$$

and representing by d_L^m any of the (L, m) coefficients of the nonlinear terms, (A 1)–(A 3) show that d_L^m is given in terms of sums like

$$\sum_{L_1, m_1} \sum_{L_2, m_2} I^{a,b,c} a_{L_1}^{m_1} a_{L_2}^{m_2}, \tag{3.12}$$

where the a_L^m's represent S_L^m, T_L^m, Θ_L^m or their radial derivatives. By a series of integrations by parts and cyclic permutations of indices,

$$I^c = \tfrac{1}{2}[L_1(L_1+1) + L_2(L_2+1) - L(L+1)]\, I^a.$$

There are essentially two ways of computing the d_L^m. The first may be termed direct evaluation, and involves computing the I's, storing them, and evaluating sums like (3.12) explicitly (see e.g. Silberman 1954; Ellsaesser 1966). The second approach is a transform method developed by Orszag (1970), and is, with a few modifications, the method used in this paper. The question of which method to use is determined by the number of harmonics kept in the expansions (2.6) and (2.7). The number of operations (an operation being defined as a multiplication followed by an addition) required for the direct evaluation of all the nonlinear terms scales as N^5 when N is large, where N is the maximum value of L retained in (2.6) and (2.7) and $-L \leqslant m \leqslant L$. The transform method scales as N^3. The storage required for both methods scales similarly when N is large. It is clear, therefore, that the transform method offers a clear advantage over direct evaluation when N is large enough. Although it is difficult to make reliable estimates of numbers of operations without doing computer counts, it was estimated that the two methods broke even somewhere between $N = 6$ and $N = 8$ for the present problem. At lower values of N, the estimated penalty for using the transform method seemed acceptable in light of the potential savings at large N. In addition to computer savings, the transform method contains a few other advantages which will be mentioned later.

Basically, the transform method of computing the nonlinear coefficients is the discrete analogue of the analytic integrations one would normally do to calculate the coefficients. A horizontal (θ, ϕ) grid structure is set up, the nonlinear terms are evaluated at each horizontal grid point, and the equivalent of a discrete integration over (θ, ϕ) performed. The fact that each of (3.11 *a–c*) is expandable in a *finite* series of surface harmonics allows the discrete method to compute exactly the nonlinear (L, m) coefficients required for (2.8)–(2.10), whereas for an arbitrary product of surface harmonics and their derivatives this would in general not be possible.

Since the transform method is described thoroughly by Orszag (1970), only the modifications that were made here will be discussed in detail. The first modification was to use Gaussian quadrature for integration over the angle θ, instead of the inverse matrices defined by Orszag. This eliminates the need to compute and store these matrices, and the only additional storage required besides the associated Legendre functions are the well-tabulated Gaussian zeros and weights. The method of Gaussian quadrature computes the nonlinear coefficients exactly, since the intergral over θ required is of the form

$$\int_{-1}^{1} g_m(\theta)\, P_n^m(\theta)\, d\mu, \tag{3.13}$$

where $\mu = \cos\theta$, $P_n^m(\theta)$ is the normalized associated Legendre function, and $g_m(\theta)$ is of the form

$$g_m(\theta) = \sum_{L \geqslant m}^{2N} d_L^m P_L^m(\theta), \tag{3.14}$$

with the product $P_n^m P_L^m$ being a polynomial in μ of degree $n+L$. For reasons discussed below, the highest degree involved in the calculations is $4N+1$, and therefore the degree of the quadrature (i.e. the value of L of the Legendre polynomial used for the quadrature) had to be greater or equal to $2N+1$. Using the fact the model is hemispheric and the zeros and weights for an even Legendre polynomial are symmetric about $\mu = 0$, only $N+1$ θ points and weights had to be used. (The use of an even-degree quadrature required using a degree $2N+2$ Legendre polynomial.)

The second significant modification to the transform method was the following. From the appendix it can be seen that the number of terms in the poloidal and toroidal equations that would have to be multiplied at each (θ, ϕ) grid point is rather large. In addition, the number of independent sums over (L, m) required at each grid point, not counting temperature, is 11. It was therefore decided to compute the nonlinear coefficients involved in (2.8) and (2.9) in the following manner. First, compute the (L, m) coefficients of

$$[(\nabla \times \mathbf{u}) \times \mathbf{u}]_r, \sin\theta[(\nabla \times \mathbf{u}) \times \mathbf{u}]_\theta, \sin\theta[(\nabla \times \mathbf{u}) \times \mathbf{u}]_\phi. \tag{3.15}$$

It is necessary to multiply by $\sin\theta$ in the last two expressions, to make the expression expandable in a finite series. The advantage of this approach is that only simple expressions are multiplied at each (θ, ϕ) grid point, and three fewer sums over (L, m) are required. This is partially balanced by the fact that coefficients all the way up to the highest in L, $2N+1$, have to be computed for the last two expressions of (3.15) (see below). One other advantage of this approach is that $\mathbf{u}$ is explicitly calculated, and this is convenient for computing the time step restriction due to the nonlinear terms.

Denoting the (L, m) components of (3.15) by $d_{r_{Lm}}$, $d_{\theta_{Lm}}$, $d_{\phi_{Lm}}$, respectively, it can be shown, after some algebra and use of recursion relations for the Y_L^m, that

$$\{\nabla \times [(\nabla \times \mathbf{u}) \times \mathbf{u}]\}_r = -\frac{1}{\sin^2\theta} \sum_{L=1}^{2N+2} \sum_{m=-L}^{L} b_{Lm} Y_L^m, \tag{3.16}$$

$$\{\nabla \times \nabla \times [(\nabla \times \mathbf{u}) \times \mathbf{u}]\}_r = \frac{1}{r\sin^2\theta} \frac{\partial}{\partial r} r \sum_{L=1}^{2N+2} \sum_{m=-L}^{L} c_{Lm} Y_L^m + \frac{1}{r} \sum_{L,m} L(L+1) d_{r_{Lm}} Y_L^m, \tag{3.17}$$

where

$$b_{Lm} = im d_{\theta_{Lm}} + (L+2) A(L+1, m) d_{\phi_{L+1,m}} - (L-1) A(L, m) d_{\phi_{L-1,m}}, \tag{3.18}$$

$$c_{Lm} = im d_{\phi_{Lm}} - (L+2) A(L+1, m) d_{\theta_{L+1,m}} + (L-1) A(L, m) d_{\theta_{L-1,m}}, \tag{3.19}$$

and

$$A(L, m) = [(L-m)(L+m)/(2L-1)(2L+1)]^{\frac{1}{2}}.$$

Because it is known from the products (3.11) that the highest L value involved in the series expansion of the left-hand sides of (3.16) and (3.17) is $2N$, we can write

$$\frac{1}{\sin^2\theta} \sum_{L,m}^{L=2N+2} b_{Lm} Y_L^m = \sum_{L,m}^{L=2N} \alpha_{Lm} Y_L^m, \tag{3.20}$$

$$\frac{1}{\sin^2\theta} \sum_{L,m}^{L=2N+2} c_{Lm} Y_L^m = \sum_{L,m}^{L=2N} \beta_{Lm} Y_L^m. \tag{3.21}$$

Using the recursion relations for the Y_L^m, we get

$$-b_{Lm} = A(L+2,m)\,A(L+1,m)\,\alpha_{L+2,m} - [1-A(L+1,m)^2-A(L,m)^2]\,\alpha_{L,m}+A(L-1,m)\,A(L,m)\,\alpha_{L-2,m}, \quad (3.22)$$

and a similar equation with c_{Lm}, β_{Lm} replacing b_{Lm}, α_{Lm}. Since $\alpha_{Lm} = 0$ for $L > 2N$, a simple recursion relation is obtained for the α_{Lm}, and similarly for the β_{Lm}. Thus all the α_{Lm}, β_{Lm} needed for (2.8) and (2.9) can be obtained. The nonlinear terms in the temperature equation as well as the $d_{r_{Lm}}$ are handled following the general procedure described by Orszag (with the exception of the Gaussian quadrature mentioned above).

Rigorous criteria for numerical stability of the present scheme could not be derived. Nevertheless, under the restrictions on the time step given below not one instance of numerical instability was encountered. The time step Δt was restricted by the minimum of the quantities

$$(N_r|u_r|_{\max})^{-1}, \quad \left(N\left|\frac{u_\theta}{r}\right|_{\max}\right)^{-1}, \quad \left(M\left|\frac{u_\phi}{r\sin\theta}\right|_{\max}\right)^{-1}, \quad \left(N_r\frac{4}{r_1}\right)^{-1}, \quad \left(\frac{N(N+1)}{r_1^2}\right)^{-1}. \quad (3.23)$$

M is the maximum value of m, usually N. The first three quantities are evaluated at each (θ, ϕ) grid point used for computation of the nonlinear terms and at each radial grid point. If $P < 1$ a factor P^{-1} appears in the last two quantities, which are derived from the remaining part of the diffusion operators after d^2/dr^2 has been subtracted out.

An idea of the computer time involved in the calculations can be obtained from the following. All computations were done on a CDC 7600. For $N \leqslant 8$, $M \leqslant 8$, $N_r = 16$, the computational time was 2·8 s per time step. When $N \leqslant 4$, $M \leqslant 4$, $N_r = 8$, 0·4 s per time step was required, and for $N \leqslant 8$, $M = 0$, $N_r = 16$, 0·28 s per time step. Most runs consisted of between 100 to 300 time steps.

4. Numerical results

All computations are done for a ratio of inner radius to outer radius, denoted by η, of either 0·3 or 0·6. Values of the Prandtl number considered are 1 and 5. The value $P = 1{\cdot}0$ is representative of most gases, while $P = 5{\cdot}0$ is large enough to show the effects of increasing P, but not so large as to make the nonlinear terms in the momentum equation unimportant. The highest value of the Rayleigh number treated is about 5·5 times the corresponding critical value.

The number of vertical levels used in all the computations was 16. Because the L value associated with the most unstable mode for the onset of convection depends on η (see figure 1), modes up to $L = 6$ were retained when $\eta = 0{\cdot}3$, and modes up to $L = 8$ were retained when $\eta = 0{\cdot}6$. For the three-dimensional solutions, $|m| \leqslant 6$ when $\eta = 0{\cdot}3$, and $|m| \leqslant 8$ when $\eta = 0{\cdot}6$. These resolutions for the fields were sufficient for accuracies of the order of 5 % for the range of R considered. The accuracy of the calculations was determined by making spot checks with different numbers of vertical levels and spherical modes.

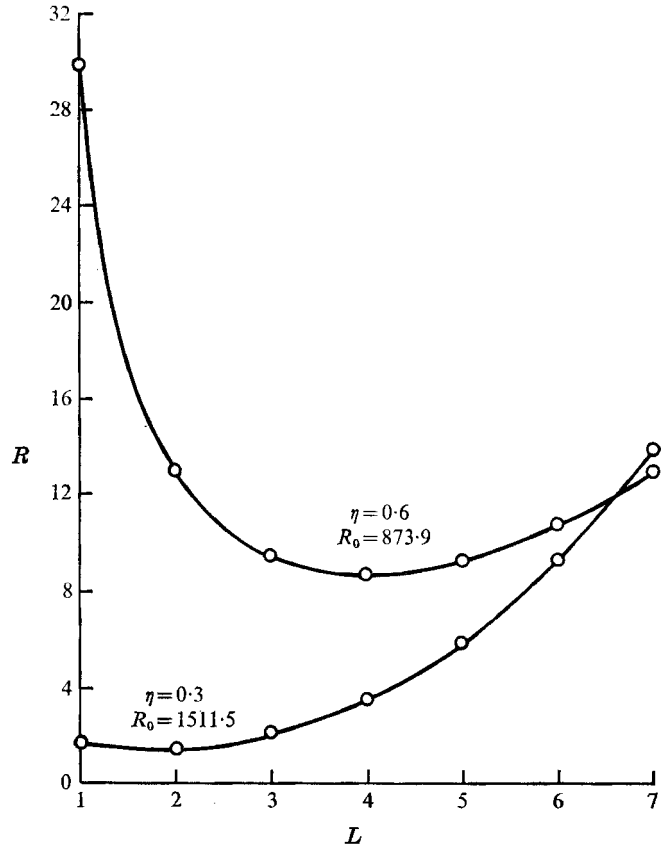

FIGURE 1. Dependence of the critical value of the Rayleigh number for the onset of convection on L. The values are determined from the formulae in Chandrasekhar (1961) using the second approximation. The ordinate should be multiplied by 10^3 for $\eta = 0{\cdot}3$ and by 10^2 for $\eta = 0{\cdot}6$.

4.1. *Axisymmetric solutions*

One result of this study is that axisymmetric solutions, the analogue of two-dimensional rolls in plane parallel convection, are not a preferred solution of the full three-dimensional equations of motion. When the initial conditions are non-axisymmetric, in general there is no tendency for the fluid motion to reduce to the axisymmetric solution, at least for values of R significantly above R_0. As discussed in § 4.2, both steady axisymmetric and non-axisymmetric solutions were obtained for the same fluid parameter values in a range of R where the axisymmetric solution appears to be stable. However, it is found that the axisymmetric solutions do become unstable above a certain value $R_c = R_c(P)$.

Stability of the axisymmetric solutions was investigated by allowing a small thermal perturbation to occur in the (L, m) modes most unstable to the onset of convection. Hence, the perturbation occurred in the $L = 2$, $m = 2$ mode for $\eta = 0{\cdot}3$, and in the $L = 4$, $m = 2$ and $m = 4$ modes when $\eta = 0{\cdot}6$. This was done rather than allowing an arbitrary or random perturbation because retaining a large number of modes would have been quite time consuming. Rigorously,

$R =$	4000	4000	8000
$P =$	1·0	5·0	5·0
S_2	−3·03	−0·701	−1·21
	−3·85	−0·928	−1·61
	−2·81	−0·628	−1·11
S_4	0·387	0·0729	0·129
	0·688	0·115	0·207
	0·521	0·0858	0·153
S_6	−0·0841	−0·0112	−0·0342
	−0·136	−0·0169	−0·0413
	−0·0895	−0·0115	−0·0238
Θ_0	−0·742	−0·153	−0·208
	−0·225	−0·0408	−0·0606
	0·106	0·0261	0·0338
Θ_2	−0·515	−0·110	−0·0917
	−0·412	−0·0855	−0·0677
	−0·302	−0·0620	−0·0631
Θ_4	0·246	0·0516	0·0522
	0·194	0·0384	0·0316
	0·121	0·0226	0·0187
Θ_6	−0·156	−0·0313	−0·0564
	−0·0901	−0·0171	−0·0194
	−0·0338	−0·00569	−0·00353

TABLE 1. Spectrum of axisymmetric solutions given at $r-r_1 = 0{\cdot}25,\ 0{\cdot}5,\ 0{\cdot}75$. $\eta = 0{\cdot}3$.

therefore, we have put only an upper bound on R_c, but it seems reasonable to expect that three-dimensional perturbations occurring in the (L, m) modes most unstable to convection will also be the perturbations determining the lowest value of R_c. The time integration was carried out until it was clear the perturbations were either decaying or growing, which sometimes required a large amount of time because of oscillatory behaviour. For this reason, R_c was determined only to the nearest 500.

When $\eta = 0{\cdot}3$ and $P = 1{\cdot}0$, the Rayleigh number above which instability occurs is between 4000 and 4500. When $\eta = 0{\cdot}6$, $P = 1{\cdot}0$, R_c lies between 1500 and 2000. However, when $P = 5{\cdot}0$ the axisymmetric solutions are stable over the whole range of R considered, both when $\eta = 0{\cdot}3$ and when $\eta = 0{\cdot}6$. It appears that there is a tendency for R_c/R_0 to decrease as η increases at fixed P, since at $P = 1{\cdot}0$ when $\eta = 0{\cdot}3$, $2{\cdot}6 \lesssim R_c/R_0 < 3$, and when $\eta = 0{\cdot}6$, $1{\cdot}8 \lesssim R_c/R_0 < 2{\cdot}4$. The possible dependence of R_c on the amplitude of a perturbation was not investigated.

Spectrum. Tables 1 and 2 illustrate the distribution of amplitude as a function of L for the velocity and temperature in various cases. It should be borne in mind when comparing amplitudes that, for example, the contribution of a mode to u_r is proportional to $L(L+1)$ times the amplitude of the mode. As expected, the dominant L mode in the solutions for the velocity is usually the L mode most unstable to the onset of convection. However, this is not always the case, as can be seen from table 2, which is for the case $P = 5{\cdot}0$, $\eta = 0{\cdot}6$. The spectrum shows

$R =$	2000	2500	4000
S_2	0·230	0·727	1·32
	0·334	1·02	1·85
	0·240	0·718	1·31
S_4	−0·416	−0·313	−0·366
	−0·569	−0·429	−0·485
	−0·395	−0·302	−0·341
S_6	−0·0111	−0·128	−0·150
	−0·00931	−0·167	−0·211
	−0·00232	−0·112	−0·153
S_8	0·0347	−0·0137	−0·0702
	0·0446	−0·0129	−0·0859
	0·0294	−0·00553	−0·0542
Θ_0	−0·151	−0·155	−0·203
	−0·0352	−0·0452	−0·0635
	0·0639	0·0616	0·0759
Θ_2	0·0309	0·0929	0·127
	0·0561	0·129	0·133
	0·0445	0·105	0·123
Θ_4	−0·133	−0·0760	−0·0620
	−0·142	−0·0780	−0·0416
	−0·117	−0·0817	−0·0639
Θ_6	−0·0128	−0·0810	−0·0521
	−0·00640	−0·0592	−0·0428
	0·00327	−0·0403	−0·0442
Θ_8	0·0573	−0·0139	−0·0498
	0·0349	−0·0105	−0·0383
	0·0175	−0·00294	−0·0214

TABLE 2. Spectrum of axisymmetric solution for $\eta = 0{\cdot}6$, $P = 5{\cdot}0$ given at $r - r_1 = 0{\cdot}25$, 0·5, 0·75.

a distinct change of character between $R = 2000$ and $R = 2500$, with the $L = 2$ mode becoming considerably larger than the mode most unstable to the onset of convection, $L = 4$. Such behaviour persisted whether the region between $R = 2000$ and $R = 2500$ was approached from above or below. This phenomenon does not occur in the steady three-dimensional solutions corresponding to the same fluid parameters, nor does it occur for axisymmetric solutions when $\eta = 0{\cdot}3$ within a similar range of R/R_0. The above comments apply also to the temperature, with the addition that at the higher values of R the $L = 0$ mode can be the largest in regions next to the boundaries where the basic temperature gradient has been modified the most by convection. Qualitatively similar effects have been observed both experimentally and theoretically in planar convection in enclosed volumes, where it is observed that the number of convection cells decreases as the Rayleigh number increases (Krishnamurti 1970; Koschmieder 1969; Davis 1968; Deardorff & Willis 1965). Whether or not the above behaviour occurs in the other solutions at higher values of R remains to be investigated.

Heat transport. Since when $P = 1{\cdot}0$ the axisymmetric solutions become

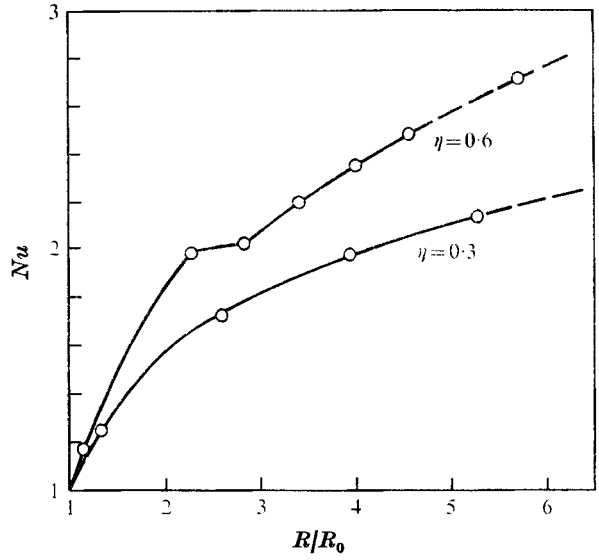

FIGURE 2. Nusselt number as a function of R/R_0 for the axisymmetric solutions at $P = 5{\cdot}0$. The last points indicated on the curve for $\eta = 0{\cdot}6$ were not checked for stability.

unstable at relatively low values of R/R_0, we shall concentrate the discussion of heat transport on the cases for which $P = 5{\cdot}0$. Figure 2 gives plots of the Nusselt number Nu against R/R_0. When $\eta = 0{\cdot}3$, the curve qualitatively resembles linear plots of Nu against R/R_0 given in Veronis (1966). Substituting in the appropriate numbers, it appears to be approaching a power law in R/R_0 with an exponent close to $\frac{1}{3}$, however, more computations would be required to establish firmly the functional dependence. When $\eta = 0{\cdot}6$, there is an inflexion region occurring between $2{\cdot}2 \lesssim R/R_0 \lesssim 2{\cdot}9$. This is in the same region of R/R_0 where the modal character of the solution is changing, as discussed previously. Transitions in Nu as a function of R/R_0 for planar convection have been observed experimentally by Malkus (1954), Willis & Deardorff (1967) and Krishnamurti (1970). Whereas they observed an increase in heat flux, in figure 2 the heat flux after the transition is less than it would have been had the transition not occurred. This is consistent with the expectation that larger cells are less efficient in transporting heat (but see Davis 1968). Krishnamurti was able to associate one transition with a change from two-dimensional rolls to three-dimensional cellular flow. From the above example, it is clear changes in the horizontal structure of two-dimensional flows can also generate transitions in heat flux. However, the transition need not be associated with the Rayleigh number at which additional horizontal modes become unstable to convection (compare the transition region of figure 2 with figure 1 at $L = 2$). Beyond the inflexion region, the curve again appears to be approaching an $(R/R_0)^n$ power law with $n \approx \frac{1}{3}$, although with a significantly different slope from when $\eta = 0{\cdot}3$. Within the range of R for which the axisymmetric solutions are stable at $P = 1{\cdot}0$, Nu is independent of P to within the accuracy of the calculations. It can be seen from figure 2 that Nu is an increasing function of η for fixed R/R_0 and P.

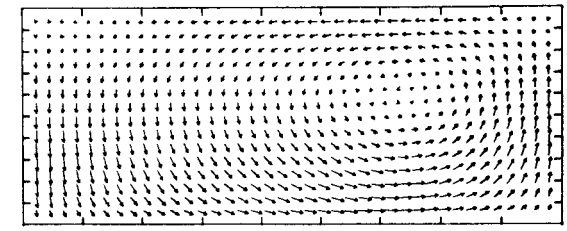

(*a*)

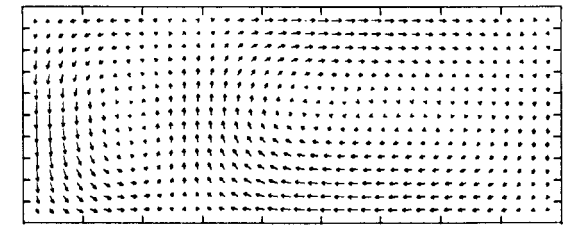

Pole (*b*) Equator

FIGURE 3. Steady-state convection cells for axisymmetric solutions. (*a*) $R = 8000$, $P = 5{\cdot}0$, $\eta = 0{\cdot}3$. (*b*) $R = 4000$, $P = 5{\cdot}0$, $\eta = 0{\cdot}6$.

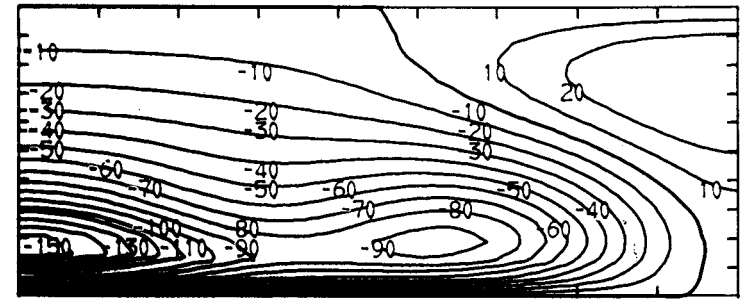

(*a*)

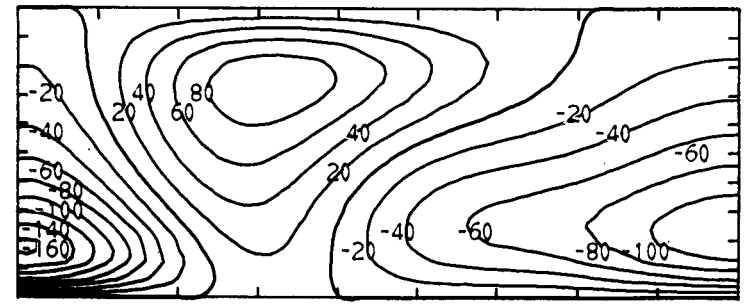

Pole (*b*) Equator

FIGURE 4. Steady-state isotherms for axisymmetric solutions. The pure conduction solution is subtracted out. The numbers in the figure represent only the relative magnitudes of the isotherms. (*a*) $R = 8000$, $P = 5{\cdot}0$, $\eta = 0{\cdot}3$. (*b*) $R = 4000$, $P = 5{\cdot}0$, $\eta = 0{\cdot}6$.

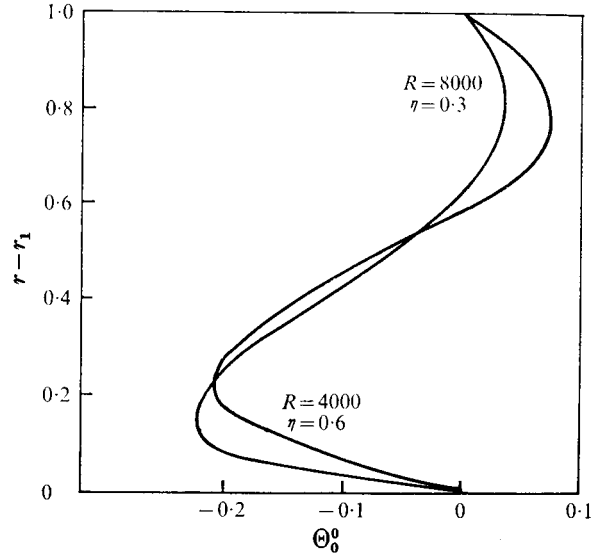

FIGURE 5. Vertical profiles of Θ_0^0. Both profiles are for $P = 5{\cdot}0$.

Velocity and temperature fields. In figures 3 and 4 are shown the steady velocity and temperature fields of two stable axisymmetric solutions. It was found that the axisymmetric solutions always reached steady state, irrespective of R or P. This is not always the case with non-axisymmetric solutions discussed in § 4.3. When $\eta = 0{\cdot}3$, figure 3 (a), there is only one cell between equator and pole, and the upwelling region is much narrower than the downwelling region. When $\eta = 0{\cdot}6$, figure 3 (b), two cells are apparent, with the cells being highly asymmetric. In both figures the asymmetric structure of the cells is partly nonlinear in origin, and partly due to the fact that the Legendre functions are only symmetric about $\theta = \frac{1}{2}\pi$. From figure 4 it can be seen that the maximum vertical thermal gradients occur near the boundaries, as expected, and are correlated with the sense of the vertical velocity. Figure 5 gives the vertical profile of the coefficient Θ_0^0 for the same cases as above.

4.2. *Non-axisymmetric solutions*

For obvious reasons non-axisymmetric solutions take much more time to obtain than do axisymmetric solutions. In addition, the approach to steady state was usually characterized by oscillatory behaviour, generally of relatively small amplitude. However, in some cases discussed later in § 4.2, the oscillations are not small and may persist indefinitely, which behaviour was never observed in the axisymmetric solutions. Toroidal modes, which are driven by nonlinear interactions involving non-axisymmetric poloidal modes, can contribute to the velocity, and must be considered. It was found, however, that toroidal modes were negligible in all but the instances of seeming permanent oscillatory behaviour mentioned above.

When $\eta = 0{\cdot}3$, the first non-axisymmetric solution was obtained by perturbing the axisymmetric solution for $R = 6000$, $P = 1{\cdot}0$ in the manner described before,

then following the time development to steady state. For reasons discussed below, when $\eta = 0{\cdot}6$ the procedure of perturbing the axisymmetric solution could not be used to obtain steady solutions at either $P = 1{\cdot}0$ or $P = 5{\cdot}0$, since the axisymmetric solutions are stable. Hence, the first non-axisymmetric solution when $\eta = 0{\cdot}6$ was obtained by subjecting the pure conduction solution to three-dimensional thermal perturbations. Once the first steady non-axisymmetric solution was obtained for either value of η, it was used as the initial conditions for solutions with different parameter values, and so on.

Duality of solutions. When $P = 5{\cdot}0$, steady non-axisymmetric as well as axisymmetric solutions were obtained up to the largest value of R considered at either value of η. Values of R as low as 1200 ($R/R_0 \cong 1{\cdot}4$) at $\eta = 0{\cdot}6$ were treated. As discussed previously, the axisymmetric solutions are stable in this range of R. The stability of the non-axisymmetric solutions is inferred from the fact that they were obtained from initial conditions differing by a finite amount from the final steady state (see also the discussion of the spectrum given below). At $P = 1{\cdot}0$, the same comments apply, except that the maximum value of R must be less than R_c to have stable axisymmetric solutions, and R must be less than $\sim 2R_0$ when $\eta = 0{\cdot}6$ to get steady non-axisymmetric solutions (see the discussion of oscillatory behaviour given later).

The fact that steady non-axisymmetric solutions exist at the same parameter values for which axisymmetric solutions were obtained indicates that axisymmetric solutions are not a preferred state of the full three-dimensional equations. Even if the steady non-axisymmetric solutions were found to be unstable to some sort of perturbation this would not alter the conclusion, since the axisymmetric modes are explicitly accounted for in the non-axisymmetric solutions, and if the solution wanted to relax to the axisymmetric case it was free to do so. In addition, none of the oscillatory solutions discussed later reduced to axisymmetry. Steady three-dimensional motions existing in regions where two-dimensional solutions are stable have been observed experimentally for planar convection by Krishnamurti (1970), who observed hysteresis effects depending on whether R_c was approached from above or below.

A comparison of the stable axisymmetric and non-axisymmetric solutions for the same fluid parameter values yields the interesting result that the Nusselt numbers differ by only $\sim 5\,\%$. This may imply that integral properties of the flow are adequately represented by the axisymmetric solutions when they are stable, even though the fields themselves are not.

In the non-axisymmetric cases there were instances where steady as well as oscillatory solutions were obtained at the same parameter values. These will be discussed later, but it is clear that initial conditions can play an important role in determining the character of the finite-amplitude solution. Of course it would be desirable to be able somehow to classify what sort of initial conditions lead to a certain kind of solution, but this just is not feasible at present because of the amount of computer time that would be required.

Spectrum. The dominant modes in the steady three-dimensional cases are the modes associated with the L value most unstable to the onset of convection. No transition regions of modal behaviour or heat flux, such as occurred in the one

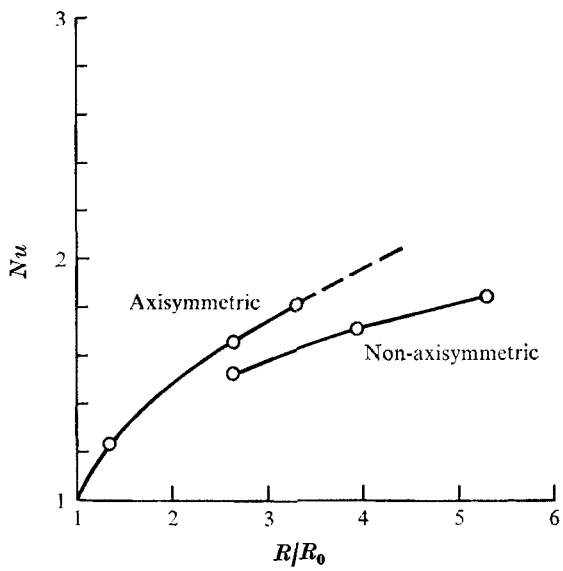

FIGURE 6. Nusselt number as a function of R/R_0. $\eta = 0{\cdot}3$, $P = 1{\cdot}0$.

axisymmetric example, were observed in any of the steady non-axisymmetric solutions for the range of R treated. Tables 3–5 present the modal distributions for three steady non-axisymmetric solutions. In each instance the value of R is the highest that was considered at the particular value of η. Note that modes with odd m values are not included. When $\eta = 0{\cdot}6$, modes with odd m values were explicitly included in the calculations, but were found to be negligible in the steady state. When $\eta = 0{\cdot}3$, as discussed above, the odd-m modes were not explicitly in the computations, since the initial conditions contained only even-m modes. Checks of stability to perturbations of odd-m modes were made in some of these cases, however, and the solutions were found to be stable. Only the oscillatory solutions discussed below had significant energy in the modes with odd values of m.

Heat transport. The dependence of heat flux on Rayleigh number for the steady non-axisymmetric solutions is similar to that of the stable axisymmetric solutions in the range of R considered, with the exception that no transition regions were observed. In other words, Nu is within about 5 % of the Nu for the stable axisymmetric cases, and is always a smoothly varying function of R/R_0. However, when the axisymmetric solution does become unstable a transition in heat flux is indicated. Figure 6 illustrates this when $\eta = 0{\cdot}3$, $P = 1{\cdot}0$. As discussed in § 4.1, the axisymmetric solution becomes unstable to non-axisymmetric perturbations when $2{\cdot}2 < R/R_0 < 2{\cdot}9$. From the figure it appears that when this happens a change of heat flux will occur if the fluid is initially in the axisymmetric state. Presumably a similar phenomenon takes place when $P = 5{\cdot}0$ when R/R_0 is large enough (i.e. at values of R/R_0 larger than those considered here, the difference in Nu between the axisymmetric and non-axisymmetric solutions is significant, and somewhere in this region the axisymmetric solution becomes unstable). Krishna-

S_2^0, S_2^2	−2·09	2·56		
	−3·30	4.04		
	−2·94	3·60		
S_4^0, S_4^2, S_4^4	0·0463	−0·0488	0·0647	
	0·148	−0·157	0·207	
	0·219	−0·231	0·306	
$S_6^0, S_6^2, S_6^4, S_6^6$	−0·00976	0·0100	−0·0110	0·0150
	−0·0235	0·0241	−0·0265	0·0360
	−0·0178	0·0182	−0·0200	0·0273
Θ_0^0	−1·01			
	−0·530			
	−0·0497			
Θ_2^0, Θ_2^2	−0·267	0·327		
	−0·168	0·206		
	−0·163	0·200		
$\Theta_4^0, \Theta_4^2, \Theta_4^4$	0·0578	−0·0610	0·0808	
	0·0641	−0·0676	0·0895	
	0·0513	−0·0541	0·0716	
$\Theta_6^0, \Theta_6^2, \Theta_6^4, \Theta_6^6$	−0·0224	0·0230	−0·0253	0·0343
	−0·0356	0·0365	−0·0400	0·0542
	−0·0169	0·0173	−0·0189	0·0257

TABLE 3. Spectrum of non-axisymmetric solution for $R = 8000$, $P = 1{\cdot}0$, $\eta = 0{\cdot}3$ at $r - r_1 = 0{\cdot}25$, $0{\cdot}5$, $0{\cdot}75$. All toroidal modes have magnitudes less than 5×10^{-3}. Modes with m odd are zero (see text).

S_2^0, S_2^2	0·598	−0·733		
	0·798	−0·978		
	0·549	−0·673		
S_4^0, S_4^2, S_4^4	0·0489	−0·0515	0·0682	
	0·0781	−0·0824	0·109	
	0·0579	−0·0610	0·0808	
$S_6^0, S_6^2, S_6^4, S_6^6$	0·0107	−0·0110	0·0120	−0·0163
	0·0130	−0·0134	0·0146	−0·0198
	0·00753	−0·00772	0·00846	−0·0115
Θ_0^0	−0·210			
	−0·0630			
	0·0314			
Θ_2^0, Θ_2^2	0·0457	−0·0560		
	0·0336	−0·0412		
	0·0311	−0·0381		
$\Theta_4^0, \Theta_4^2, \Theta_4^4$	0·0197	−0·0267	0·0274	
	0·0120	−0·0127	0·0168	
	0·00718	−0·00750	0·00993	
$\Theta_6^0, \Theta_6^2, \Theta_6^4, \Theta_6^6$	0·0177	−0·0181	0·0198	−0·0268
	0·00614	−0·00629	0·00689	−0·00933
	0·00115	−0·00118	0·00129	−0·00174

TABLE 4. Spectrum of non-axisymmetric solution for $R = 8000$, $P = 5{\cdot}0$, $\eta = 0{\cdot}3$ at $r - r_1 = 0{\cdot}25$, $0{\cdot}5$, $0{\cdot}75$. All toroidal modes have magnitudes less than 10^{-4}. Modes with m odd are zero.

S_2^0, S_2^2	−0·00294	0·00111			
	−0·00452	0·00176			
	−0·00363	0·00141			
S_4^0, S_4^2, S_4^4	−0·130	0·411	0·234		
	−0·192	0·606	0·344		
	−0·146	0·460	0·262		
$S_6^0, S_6^2, S_6^4, S_6^6$	0·00648	0·00103	−0·00225	0·00182	
	−0·0197	−0·0101	0·0172	−0·0137	
	−0·0307	−0·0139	0·0241	−0·0192	
$S_8^0, S_8^2, S_8^4, S_8^6, S_8^8$	0·0201	−0·00857	0·0205	0·0197	0·0113
	0·0250	−0·0106	0·0254	0·0244	0·0140
	0·0155	−0·00659	0·0157	0·0151	0·00867
Θ_0^0	0·221				
	−0·110				
	0·0471				
Θ_2^0, Θ_2^2	$6{\cdot}80 \times 10^{-5}$	$-8{\cdot}4 \times 10^{-5}$			
	$-2{\cdot}12 \times 10^{-4}$	$7{\cdot}4 \times 10^{-5}$			
	$-6{\cdot}24 \times 10^{-4}$	$2{\cdot}37 \times 10^{-4}$			
$\Theta_4^0, \Theta_4^2, \Theta_4^4$	−0·0213	0·0682	0·0385		
	−0·0213	0·0674	0·0383		
	−0·0252	0·0793	0·0452		
$\Theta_6^0, \Theta_6^2, \Theta_6^4, \Theta_6^6$	0·0127	0·00432	−0·00777	0·00618	
	−0·00775	−0·00351	0·00613	−0·00490	
	−0·0109	−0·00466	0·00811	−0·00646	
$\Theta_8^0, \Theta_8^2, \Theta_8^4, \Theta_8^6, \Theta_8^8$	0·0237	−0·0102	0·0243	0·0232	0·0134
	0·0146	−0·00626	0·0149	0·0143	0·00823
	−0·00142	$6{\cdot}87 \times 10^{-4}$	−0·00158	−0·00141	$-8{\cdot}91 \times 10^{-4}$

TABLE 5. Spectrum of non-axisymmetric solution for $R = 4000$, $P = 5{\cdot}0$, $\eta = 0{\cdot}6$ at $r - r_1 = 0{\cdot}25$, $0{\cdot}5$, $0{\cdot}75$. All toroidal modes and modes with m odd have magnitudes less than 5×10^{-3}.

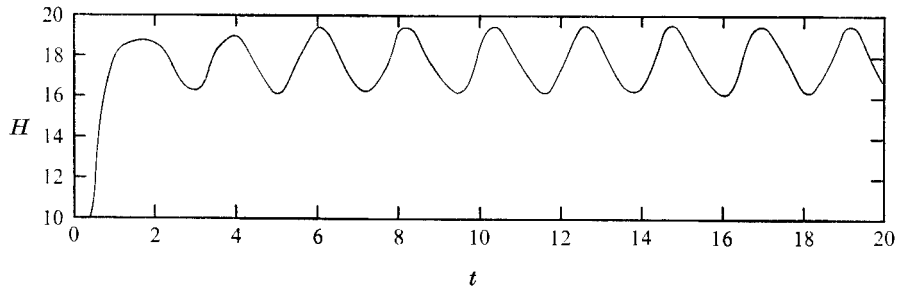

FIGURE 7. Temporal behaviour of the net conductive heat flux H at the inner boundary for the oscillatory case $R = 2500$, $P = 5{\cdot}0$, $\eta = 0{\cdot}6$.

murti (1970) has observed experimentally a transition in dependence of heat flux on Rayleigh number for planar convection associated with the instability of two-dimensional rolls to three-dimensional disturbances.

Oscillatory behaviour. As discussed already, once a steady non-axisymmetric solution was obtained, it could be used as the initial conditions for subsequent

calculations at neighbouring parameter values. In this manner were most of the steady solutions computed. However, starting from different initial conditions, a steady state was not always achieved at the same parameter values for which a steady solution was obtained by the method described above. Such a case is $R = 2500$, $P = 5{\cdot}0$, $\eta = 0{\cdot}6$, for which computations were also made using as initial conditions non-axisymmetric thermal perturbations to the pure conduction solution. For the most part, these computations were done using the representation $N \leqslant 4, m \leqslant 4, N_r = 8$, because the highly oscillatory nature of the flow precluded making lengthy runs with more accurate representations owing to the very large amount of computer time that would have been required. Figure 7 illustrates the variation of the total heat flux at the lower boundary as a function of time. Once the initial transient period is over, the dependence settles down to an essentially sinusoidal oscillation. The oscillation periods for the poloidal and thermal modes were generally about 1·5 times the oscillation period of figure 7, while the toroidal modes had oscillations having approximately twice this period. This behaviour was verified by integrating over one oscillation period of figure 7 with the representation $N \leqslant 8, m \leqslant 8, N_r = 16$. The period of oscillation was virtually unchanged, and the amplitude of the oscillation increased by approximately 15 %. Therefore, whether or not a solution reaches steady state appears to depend on the initial conditions from which it is started.

In addition, when $P = 1{\cdot}0$, $\eta = 0{\cdot}6$, no steady solutions at all could be found when $R/R_0 \gtrsim 2$. At $R/R_0 = 1{\cdot}37$ ($R = 1200$) a steady solution exists, and when $P = 5{\cdot}0$ steady solutions were obtained up to the maximum value of R treated, $R/R_0 \sim 4$. When $\eta = 0{\cdot}3$ steady solutions could be obtained when $P = 1{\cdot}0$ over the entire range of R considered (i.e. up to $R/R_0 \sim 5$). Therefore, it can be speculated that as η increases one must go to larger values of P and/or smaller values of R/R_0 for steady non-axisymmetric solutions to exist.

The fact that toroidal modes are significant in the oscillatory solutions but quite small in the steady cases suggests that the origin of the oscillatory behaviour lies in the nonlinear terms of the momentum equation. This conclusion is supported by the fact that steady non-axisymmetric solutions could not be found at all when $\eta = 0{\cdot}6$, $P = 1{\cdot}0$, $R/R_0 \gtrsim 2$, but were obtained at $P = 5{\cdot}0$ for $R/R_0 > 2$. If P is taken as very large so that the nonlinear terms in the momentum equation become much less important, it is possible that oscillatory behaviour would not occur for any set of initial conditions. As mentioned previously, the axisymmetric solutions always reached steady state, irrespective of the values of R or P, with toroidal modes not occurring in these solutions because there is nothing to drive them.

Velocity and temperature fields. Of particular interest concerning the steady non-axisymmetric solutions is the horizontal planform of the convection cells. Figure 8 illustrates the horizontal velocity field at the outer boundary using a polar stereographic projection. When $\eta = 0{\cdot}3$, $P = 1{\cdot}0$, $R = 8000$, figure 8(*a*) shows two cells, with the centre of each cell located on the equator; fluid rises at the centre and descends over a rather broad region which more or less defines the cell boundaries. Located 90° in longitude away from the centres of rising fluid are null points where the total fluid velocity is very small. Surprisingly, when

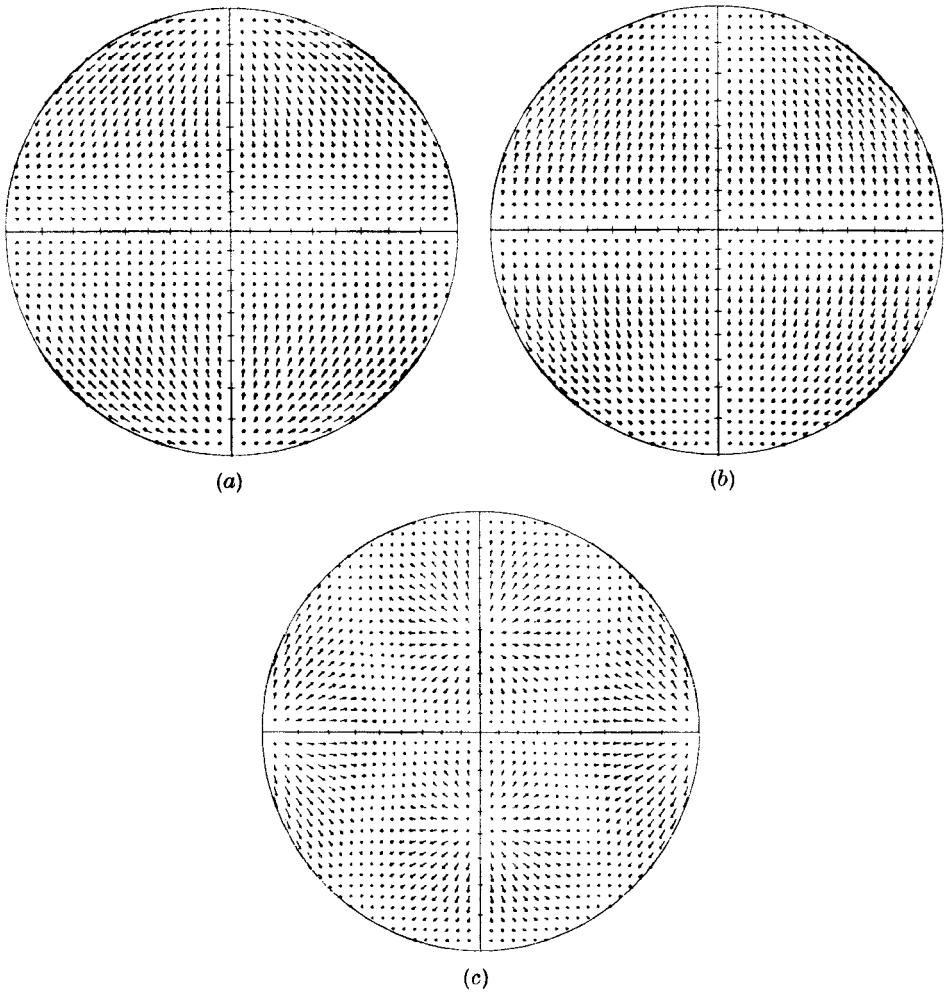

FIGURE 8. Steady horizontal velocity field at the upper boundary using a polar stereographic projection. The bottom point of the figure corresponds to $\phi = 0$. (*a*) $R = 8000$, $P = 1{\cdot}0$, $\eta = 0{\cdot}3$. (*b*) $R = 8000$, $P = 5{\cdot}0$, $\eta = 0{\cdot}3$. (*c*) $R = 4000$, $P = 5{\cdot}0$, $\eta = 0{\cdot}6$.

$P = 5{\cdot}0$ for the same values of η and R, figure 8(*b*), the descending and rising regions have switched positions, so that the centre of the cell is now associated with downwelling fluid.

Figure 8(*c*) illustrates the case $\eta = 0{\cdot}6$, $P = 5{\cdot}0$, $R = 4000$. Four cells can be seen, which means that a total of six cells occur over the whole sphere (remember that the flow is symmetric about the equator). The cells are somewhat distorted towards the equator by the projection, but by carefully comparing latitudes, or by looking at figure 9(*c*), it can be seen that the cells not located on the equator extend almost equally in latitude on either side of the cell centre, which is located at $\theta = 45°$. Again there are null points located 90° in longitude away from the centres of the equatorial cells.

Figures 9 and 10 present meridional cross-sections of $\mathbf{u}$ and Θ for the same

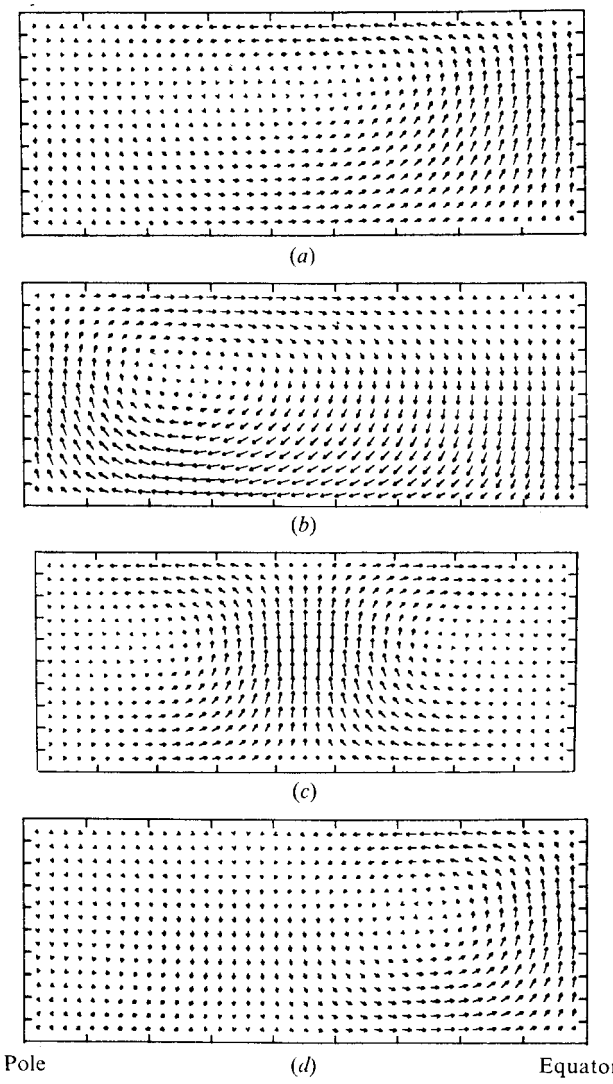

FIGURE 9. Meridional cross-section of the steady convection cells. (*a*) $R = 8000$, $P = 1{\cdot}0$, $\eta = 0{\cdot}3$, $\phi = 0$. (*b*) Same as (*a*), except $P = 5{\cdot}0$. (*c*) $R = 4000$, $P = 5{\cdot}0$, $\eta = 0{\cdot}6$, $\phi = 0$. (*d*) Same as (*c*), except $\phi = \frac{1}{2}\pi$.

cases as in figure 8. In most of the figures the magnitude of the vertical velocity is considerably greater in the upwelling regions than in the descending regions, the descending regions being spread over a relatively broad area. The exception is the case $P = 5{\cdot}0$, $R = 8000$, $\eta = 0{\cdot}3$, figure 9(*b*), where the up and downwelling velocities are comparable. As in the axisymmetric cases, the largest values of vertical thermal gradient occur near the boundaries, and are clearly correlated with the sign of the vertical velocity. Figure 11 presents the vertical profiles of the coefficient Θ_0^0.

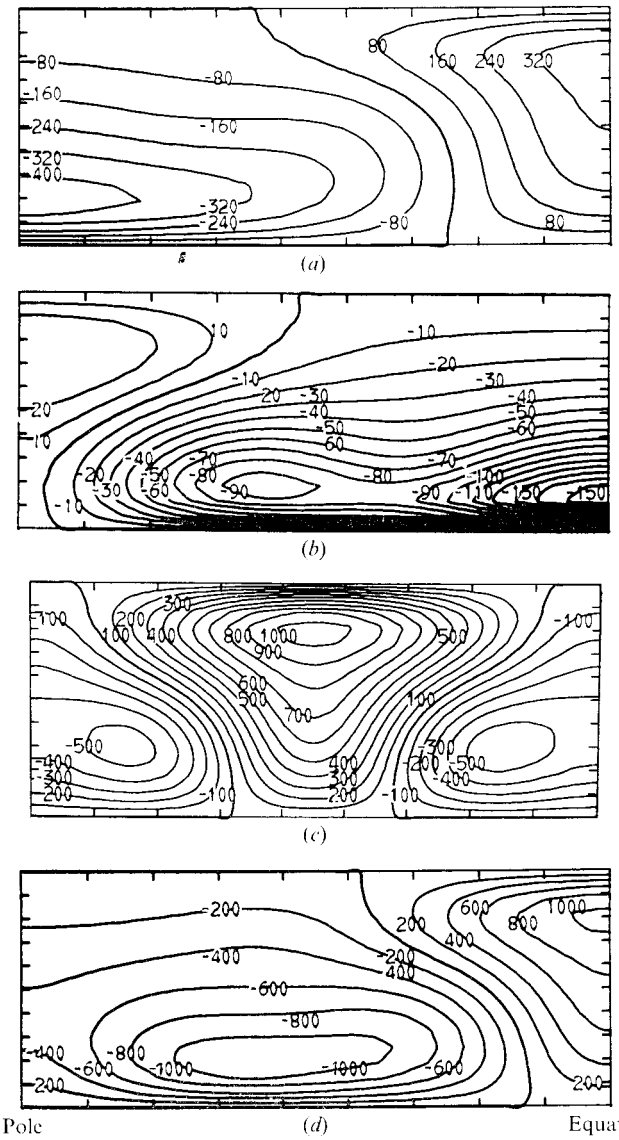

FIGURE 10. Meridional cross-section of the steady temperature fields. The pure conduction solution is subtracted out. The numbers in the figure represent only the relative magnitudes of the isotherms. (*a*) $R = 8000$, $P = 1{\cdot}0$, $\eta = 0{\cdot}3$, $\phi = 0$. (*b*) Same as (*a*), except $P = 5{\cdot}0$. (*c*) $R = 4000$, $P = 5{\cdot}0$, $\eta = 0{\cdot}6$, $\phi = 0$. (*d*) Same as (*c*) except $\phi = \frac{1}{2}\pi$.

5. Discussion and conclusions

Two major results emerging from the computations are that initial conditions are important in determining the finite-amplitude behaviour of the fluid, and second, that a range of R exists where axisymmetric solutions are stable but are not preferred; in other words, if for this range of R the initial conditions are non-axisymmetric, there is no tendency for the fluid to reduce to an axisymmetric state. Some of the experimental observations of Krishnamurti (1970) indicate

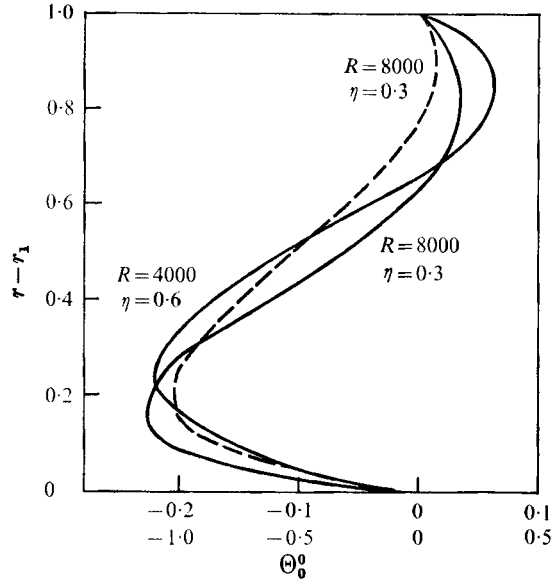

FIGURE 11. Vertical profiles of Θ_0^0. —, $P = 5{\cdot}0$, – – –, $P = 1{\cdot}0$. The bottom scale is for $P = 1{\cdot}0$.

there may be similar behaviour in planar convection, with three-dimensional cellular convection occurring in the region of R where two-dimensional rolls are stable.

The fact that initial conditions are important in planar convection is indicated by the work of Schlüter, Lortz & Busse (1965) and Busse (1967), and has been explicitly demonstrated by Foster (1969) and Ogura (1971). In this work the dependence on initial conditions has been demonstrated for the non-axisymmetric solutions. In particular, it was found that depending on initial conditions it is possible for both steady and oscillatory solutions to exist at the same parameter values. In addition, as described above, both stable non-axisymmetric and axisymmetric solutions can exist at the same parameter values.

Computations regarding stability show that steady axisymmetric solutions become unstable to small non-axisymmetric disturbances above a certain value of the Rayleigh number, and this value is an increasing function of Prandtl number. Such behaviour is in qualitative agreement with the results of Busse (1972) concerning the instability of two-dimensional rolls to three-dimensional perturbations at small values of the Prandtl number.

The dominant modes in the solutions are usually the modes most unstable to the onset of convection. However, as the Rayleigh number is increased, a sudden transition in horizontal flow structure occurs in the stable axisymmetric case for which $\eta = 0{\cdot}6$, $P = 5{\cdot}0$ (i.e. the dominant mode changes from one corresponding to a value $L = 4$ to one corresponding to a value $L = 2$). Associated with this change in modal behaviour is a transition in the dependence of heat flux on R which occurs within a range of R that is significantly above the value at which the $L = 2$ mode becomes unstable to the onset of convection, indicating that the transition is not associated with new modes becoming unstable. Such behaviour

was not observed in any of the non-axisymmetric solutions, but presumably at high enough values of R similar transitions would occur. However, there does apparently exist a transition in heat flux when the axisymmetric solutions become unstable and the fluid is initially in the axisymmetric state.

Finally, when $\eta = 0{\cdot}6$, $P = 1{\cdot}0$, steady non-axisymmetric solutions could not be found for $R/R_0 \gtrsim 2$, whereas when $\eta = 0{\cdot}6$, $P = 5{\cdot}0$, or $\eta = 0{\cdot}3$, $P = 1{\cdot}0$ steady solutions could be obtained for $R/R_0 > 2$. This does not prove steady solutions do not exist when $\eta = 0{\cdot}6$, $P = 1{\cdot}0$, $R/R_0 \gtrsim 2$, since computations were not made starting from all possible initial conditions. Nevertheless, the implication is that, as η increases, stable steady solutions become possible only as the Prandtl number increases and/or the Rayleigh number decreases.

Unfortunately, a number of interesting questions have been left unanswered by the present study, because of the practical consideration of computer time. For example, in the case of the axisymmetric solutions it would be desirable to generate the actual curve $R_c = R_c(P)$ and to investigate further possible transitions in horizontal flow structure and heat flux. Also, the effects of initial conditions on axisymmetric solutions need to be considered. Concerning the non-axisymmetric solutions, one would like to determine the relationship between R and P that defines the region where steady solutions exist, and in addition to determine a similar curve where steady solutions are the only ones that exist, assuming there is such a curve. Where do transitions in flow structure and heat flux occur in three dimensions? And finally, as $\eta \to 1$, do axisymmetric solutions become preferred solutions?

The author benefited from numerous discussions with Bernard Durney, Peter Gilman and Jack Herring. Many thanks are also due David Gubbins for his detailed and constructive comments on the preliminary draft of the paper. The work was carried out at the National Center for Atmospheric Research, which is sponsored by the National Science Foundation.

Appendix

The nonlinear terms involved in the toroidal, poloidal and temperature equations are given below in terms of products of spherical surface harmonics. We shall denote the products (3.11*a–c*) by P_1, P_2, P_3, respectively. In addition, a summation over L_1, m_1, L_2, m_2 is always implied, so the summation signs will be omitted.

$$\begin{aligned}\hat{\mathbf{r}}.\nabla\times[(\nabla\times\mathbf{u})\times\mathbf{u}] = {}& \frac{1}{r^3}L_1(L_1+1)\frac{\partial}{\partial r}(r^2T^{m_1}_{L_1})\,S^{m_2}_{L_2}L_2(L_2+1)\,P_1\\ & -\frac{1}{r^2}L_1(L_1+1)\,T^{m_1}_{L_1}\frac{\partial}{\partial r}(rS^{m_2}_{L_2})\,L_2(L_2+1)\,P_1 - T^{m_1}_{L_1}T^{m_2}_{L_2}L_2(L_2+1)\,P_2\\ & +\frac{1}{r^2}L_1(L_1+1)\,S^{m_1}_{L_1}\mathscr{D}_{L_2}S^{m_2}_{L_2}P_2\\ & +\frac{1}{r^2}L_1(L_1+1)\,T^{m_1}_{L_1}\frac{\partial}{\partial r}(rS^{m_2}_{L_2})\,P_3 - \frac{1}{r^3}L_1(L_1+1)\,S^{m_1}_{L_1}\frac{\partial}{\partial r}(r^2T^{m_2}_{L_2})\,P_3,\end{aligned} \tag{A 1}$$

$$\begin{aligned}\hat{\mathbf{r}}.\nabla<\nabla\times[(\nabla\times\mathbf{u})\times\mathbf{u}] = &-\frac{1}{r^2}\frac{\partial}{\partial r}\Big\{r^2L_1(L_1+1)\,T^{m_1}_{L_1}L_2(L_2+1)\,T^{m_2}_{L_2}P_1\\
&+L_1(L_1+1)\,\mathscr{D}_{L_1}S^{m_1}_{L_1}L_2(L_2+1)\,S^{m_2}_{L_2}P_1\\
&+T^{m_1}_{L_1}L_1(L_1+1)\frac{\partial}{\partial r}(rS^{m_2}_{L_2})\,P_2-\frac{1}{r}L_1(L_1+1)\,S^{m_1}_{L_1}\frac{\partial}{\partial r}(r^2T^{m_2}_{L_2})\,P_2\\
&-r^2L_1(L_1+1)\,T^{m_1}_{L_1}T^{m_2}_{L_2}P_3-L_1(L_1+1)\,S^{m_1}_{L_1}\mathscr{D}_{L_2}S^{m_2}_{L_2}P_3\Big\}\\
&-\frac{1}{r^2}\mathscr{L}^2\Big[rT^{m_1}_{L_1}\mathscr{D}_{L_2}S^{m_2}_{L_2}P_2+\frac{1}{r^2}\frac{\partial}{\partial r}(r^2T^{m_1}_{L_1})\frac{\partial}{\partial r}(rS^{m_2}_{L_2})\,P_2\\
&-\frac{1}{r}\mathscr{D}_{L_1}S^{m_1}_{L_1}\frac{\partial}{\partial r}(rS^{m_2}_{L_2})\,P_3-\frac{\partial}{\partial r}(r^2T^{m_1}_{L_1})\,T^{m_2}_{L_2}P_3\Big],\end{aligned}\tag{A 2}$$

where

$$\mathscr{L}^2=\frac{1}{\sin\theta}\frac{\partial}{\partial\theta}\left(\sin\theta\frac{\partial}{\partial\theta}\right)+\frac{1}{\sin^2\theta}\frac{\partial^2}{\partial\phi^2},$$

$$\mathbf{u}.\nabla\Theta=\frac{L_1(L_1+1)}{r}S^{m_1}_{L_1}\frac{\partial\Theta^{m_2}_{L_2}}{\partial r}P_1-T^{m_1}_{L_1}\Theta^{m_2}_{L_2}P_2+\frac{1}{r^2}\frac{\partial}{\partial r}(rS^{m_1}_{L_1})\,\Theta^{m_2}_{L_2}P_3.\tag{A 3}$$

REFERENCES

Busse, F. H. 1967 *J. Math. & Phys.* **46**, 140.

Busse, F. H. 1972 *J. Fluid Mech.* **52**, 97.

Chandrasekhar, S. 1961 *Hydrodynamic and Hydromagnetic Stability*. Oxford: Clarendon Press.

Condon, E. U. & Shortley, G. H. 1951 *The Theory of Atomic Spectra*. Cambridge University Press.

Cooley, J. W., Lewis, P. A. & Welch, P. D. 1970 *J. Sound Vib.* **12**, 315.

Davis, S. 1968 *J. Fluid Mech.* **32**, 619.

Deardorff, J. W. & Willis, G. E. 1965 *J. Fluid Mech.* **23**, 337.

Durney, B. 1968 *J. Atmos. Sci.* **25**, 372.

Ellsaesser, H. W. 1966 *J. Appl. Meteor.* **5**, 246.

Foster, T. D. 1969 *J. Fluid Mech.* **37**, 81.

Holloway, J. L., Spelman, M. J. & Manabe, S. 1973 *Mon. Wea. Rev.* **101**, 69.

Jackson, J. D. 1962 *Classical Electrodynamics*. Wiley.

Koschmieder, E. L. 1969 *J. Fluid Mech.* **35**, 527.

Krishnamurti, R. 1970 *J. Fluid Mech.* **42**, 295.

Malkus, W. V. R. 1954 *Proc. Roy. Soc.* A **225**, 185.

Morse, P. M. & Feshbach, H. 1953 *Methods of Theoretical Physics*. McGraw-Hill.

Ogura, Y. 1971 *J. Atmos. Sci.* **28**, 709.

Orszag, S. A. 1970 *J. Atmos. Sci.* **27**, 890.

Schlüter, A., Lortz, D. & Busse, F. H. 1965 *J. Fluid Mech.* **23**, 129.

Silberman, I. 1954 *J. Appl. Meteor.* **11**, 27.

Veronis, G. 1966 *J. Fluid Mech.* **26**, 49.

Westlake, J. R. 1968 *A Handbook of Numerical Matrix Inversion and Solution of Linear Equations*. Wiley.

Willis, G. E. & Deardorff, J. W. 1967 *Phys. Fluids*, **10**, 1861.